Nessun Dorma, a novel centralspindlin partner, is required for cytokinesis in *Drosophila* spermatocytes

Emilie Montembault,[1,2] Wei Zhang,[3] Marcin R. Przewloka,[2] Vincent Archambault,[2] Emeric W. Sevin,[4] Ernest D. Laue,[3] David M. Glover,[2] and Pier Paolo D'Avino[1,2]

[1]Department of Pathology, [2]Cancer Research UK, Cell Cycle Genetics Research Group, Department of Genetics, and [3]Department of Biochemistry, University of Cambridge, Cambridge CB2 1QP, England, UK
[4]European Bioinformatics Institute, European Molecular Biology Laboratory, Wellcome Trust Genome Campus Hinxton, Cambridge CB10 1SD, England, UK

Cytokinesis, the final step of cell division, usually ends with the abscission of the two daughter cells. In some tissues, however, daughter cells never completely separate and remain interconnected by intercellular bridges or ring canals. In this paper, we report the identification and analysis of a novel ring canal component, Nessun Dorma (Nesd), isolated as an evolutionarily conserved partner of the centralspindlin complex, a key regulator of cytokinesis. Nesd contains a pectin lyase–like domain found in proteins that bind to polysaccharides, and we present evidence that it has high affinity for β-galactosides in vitro. Moreover, *nesd* is an essential gene in *Drosophila melanogaster*, in which it is required for completion of cytokinesis during male meiosis and possibly in female germline cells. Our findings indicate that Nesd is a novel carbohydrate-binding protein that functions together with centralspindlin in late cytokinesis, thus highlighting the importance of glycosylation in this process.

Introduction

In a typical symmetric division of an animal cell, a cleavage furrow forms at the equator after chromosome segregation and ingresses to bisect the mother cell. At the same time, an array of antiparallel and interdigitating microtubules, known as the central spindle (CS), is assembled between the segregating chromosomes. Cleavage furrow ingression is usually driven by the assembly and contraction of actomyosin subcortical filaments that form a contractile ring (CR) at the cleavage site. The CR interacts with the plasma membrane, leading to its invagination during furrowing. After CR constriction, the CS forms a compact structure within the intercellular bridge known as the midbody, which contains at its center a phase-dense structure, the midbody ring or Flemming body. This structure is composed of CR and CS proteins and serves as a platform for the delivery of membrane vesicles and the recruitment of mitotic regulators during the final abscission of the two daughter cells (Otegui et al., 2005; Eggert et al., 2006).

The CS and its associated proteins control many processes during cytokinesis, including cleavage plane positioning, CR constriction, and cell abscission (D'Avino et al., 2005; Prekeris and Gould, 2008). Among these CS-associated proteins, a prominent role is played by the evolutionarily conserved centralspindlin complex, which is composed of a plus end–directed kinesin 6 protein, dubbed MKLP1 in mammals and Pavarotti kinesin-like protein (Pav-KLP) in *Drosophila melanogaster*, and a Rho family GTPase-activating protein (GAP), known as RacGAP1 in mammals and RacGAP50C/Tum in flies (Adams et al., 1998; Hirose et al., 2001; Mishima et al., 2002; Somers and Saint, 2003). This complex regulates several processes during cytokinesis by interacting with different proteins. Upon binding a Rho guanine exchange factor, known as Pebble in flies and ECT2 in mammals, it can activate the small GTPase RhoA and thus promote assembly and contraction of the actomyosin filaments of the CR (Somers and Saint, 2003; Yüce et al., 2005). Moreover, interaction of its RacGAP component with the actomyosin-binding protein Anillin serves to establish a direct link between the CR and the CS during furrow ingression (D'Avino et al., 2008;

Correspondence to Pier Paolo D'Avino: ppd21@hermes.cam.ac.uk

V. Archambault's present address is Institut de Recherche en Immunologie et en Cancérologie, Université de Montréal, Montréal, Québec H3C 3J7, Canada.

Abbreviations used in this paper: CR, contractile ring; CS, central spindle; DIC, differential interference contrast; dsRNA, double-stranded RNA; GAP, GTPase-activating protein; Hts, hu-li tai shao; MS, mass spectrometry; Nesd, Nessun Dorma; NHD, Nesd homology domain; Pav-KLP, Pavarotti kinesin-like protein; PH, pleckstrin homology; PLD, pectin lyase–like domain; PrA, protein A.

The Rockefeller University Press $30.00
J. Cell Biol. Vol. 191 No. 7 1351–1365
www.jcb.org/cgi/doi/10.1083/jcb.201007060

Gregory et al., 2008). Finally, recent studies indicate that centralspindlin could also mediate the targeting of recycling endosomes to the midbody and participate in abscission through its association with the Rab11-interacting protein FIP3 and Cep55 (Zhao et al., 2006; Simon et al., 2008).

Although many cytokinesis mechanisms are common to different cell types, abscission can be optional and depends on the tissue and developmental context. In *Drosophila* and other organisms, stable intercellular bridges, also called ring canals, are often established after incomplete cytokinesis and maintain a connection between cells in some tissues (Spradling, 1993; Hime et al., 1996; Robinson and Cooley, 1996). The occurrence of ring canals is well documented in male and female germline cells especially in *Drosophila*, in which they allow synchronous divisions and differentiation of the cells from the same cyst. These cells undergo typical cytokinesis but do not complete abscission; the CR does not fully close and is instead modified in a stable ring canal. Thus, during oogenesis and spermatogenesis, gametes develop as syncytial cells. After asymmetric division of a germline stem cell, a founder cell called gonial cell in males or cystoblast in females undergoes four rounds of mitotic divisions to produce a cyst of 16 germ cells. Cytokinesis is incomplete during these divisions, and 15 ring canals separate 16 primary spermatocytes in males or 15 nurse cells and the oocyte in females. In males, two additional rounds of ring canal formation occur during the two meiotic divisions to form cysts of 64 haploid spermatids interconnected by 63 ring canals (Fuller, 1993; Spradling, 1993).

In this article, we report the identification and analysis of a novel ring canal component, dubbed Nessun Dorma (Nesd), which was identified as a new partner of the centralspindlin complex in *Drosophila* cultured cells. Nesd can interact with both centralspindlin components in vivo and in vitro and accumulate at the midbody ring in late cytokinesis, where it colocalizes with Pav-KLP and RacGAP50C. We further show that Nesd structure, localization, and interaction with centralspindlin have been conserved in human cells. Nesd contains a putative carbohydrate-binding motif and displays high affinity for β-galactosides in vitro. Finally, we show that Nesd accumulates at ring canals in *Drosophila* and is required for completion of cytokinesis and ring canal formation during male meiosis and in female germ cells.

Results

Nesd interacts with centralspindlin in vivo and in vitro

To unravel new potential functions of the centralspindlin complex during cytokinesis, we attempted to identify its partners in *Drosophila* cultured S2 cells using an affinity purification methodology we recently established (D'Avino et al., 2009). Both components of the complex, Pav-KLP and RacGAP50C, were tagged with two IgG-binding domains of protein A (PrA) and stably expressed in *Drosophila* cells. The tagged baits were then affinity purified along with their interacting proteins, and all the components were identified by mass spectrometry (MS). As expected, each centralspindlin component was able to pull down its respective partner (i.e., Pav-KLP pulled down RacGAP50C and vice versa; Fig. 1 A). Interestingly, we also isolated with a very high score in both purifications a novel, uncharacterized protein annotated as CG10722 in the *Drosophila* database. We dubbed this novel centralspindlin interactor "Nessun Dorma" after Pavarotti's most famous aria from the opera Turandot (Fig. 1 A). A reciprocal pull-down assay using PrA-tagged Nesd was used to confirm this interaction in cultured cells (Fig. 1 B). To investigate whether Nesd interacted directly with centralspindlin components in vitro, we tested the ability of a recombinant GST-tagged Nesd to pull down Pav-KLP and RacGAP50C fragments translated and labeled in vitro with [^{35}S]methionine. Both centralspindlin components were found to interact in vitro with GST::Nesd, and this interaction did not require the GAP domain of RacGAP50C or the motor domain of Pav-KLP (Fig. 1 C). Consistent with this, recombinant GST-tagged full-length RacGAP50C and Pav-KLP proteins were also able to pull down in vitro translated and radiolabeled Nesd in a reciprocal experiment (Fig. S1 A). To narrow down the regions in both centralspindlin components able to interact with Nesd, we tested the ability of several RacGAP50C and Pav-KLP fragments to bind to GST::Nesd in vitro. Our pull-down results indicated that Nesd was able to bind directly to the RacGAP50C$_{136–240}$ region and to the central stalk domain of Pav-KLP (Pav$_{461–685}$). The RacGAP50C$_{136–240}$ fragment was not known to harbor binding sites for any of the other RacGAP50C interactors (Anillin, Pebble, and Pav-KLP; Somers and Saint, 2003; D'Avino et al., 2008; Gregory et al., 2008), whereas the stalk domain of the human Pav-KLP counterpart MKLP1 is important for its interaction with MgcRacGAP and Cep55 (Zhao et al., 2006; Pavicic-Kaltenbrunner et al., 2007).

Nesd localizes to the midbody and interacts with centralspindlin via its conserved N-terminal region

We raised a polyclonal antibody to investigate Nesd subcellular localization. Western blot analysis of S2 cell extracts revealed a specific band of the expected size (~65 kD), which was drastically reduced after *nesd* RNAi treatment (Fig. 2 A). Nesd was detected by immunofluorescence at the midbody and intercellular bridge in late cytokinesis in S2 cells, even after disassembly of the CS microtubules (Fig. 2 B). The signal at the midbody was specific because it disappeared after *nesd* RNAi treatment (Fig. S1 B). Nesd colocalized with both Pav-KLP and RacGAP50C but only in late telophase (Figs. 2 C and S1 C). Nesd tagged with the GFP displayed an almost identical localization pattern, although a faint signal could also be detected on CS microtubules in early telophase (Fig. 2 D). We never observed such localization in early telophase using our Nesd antibody, and, thus, we cannot exclude that this distribution could be the result of overexpressing the GFP-tagged protein. However, it is also possible that our antibody might not be able to detect low levels of Nesd protein during the early stages of furrowing.

Nesd sequence analysis identified two potential domains: a highly conserved region in the N-terminal half of the protein, which we dubbed Nesd homology domain (NHD; Nesd$_{30–212}$), and a pectin lyase–like domain (PLD; Nesd$_{334–574}$) in the C-terminal half (Fig. 2 F). This latter motif, characterized by a series of

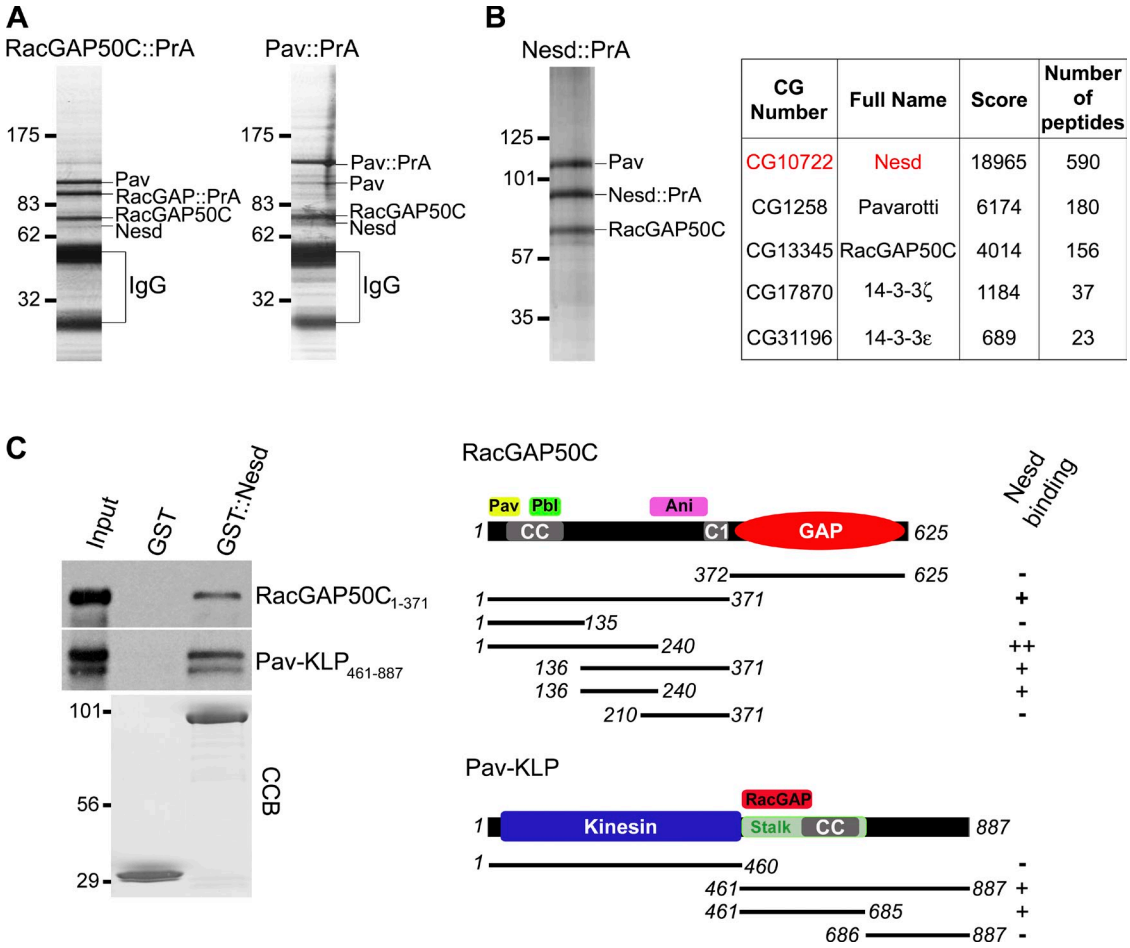

CG Number	Full Name	Score	Number of peptides
CG10722	Nesd	18965	590
CG1258	Pavarotti	6174	180
CG13345	RacGAP50C	4014	156
CG17870	14-3-3ζ	1184	37
CG31196	14-3-3ε	689	23

Figure 1. **Nesd interacts with both centralspindlin components in vivo and in vitro.** (A) Colloidal Coomassie blue–stained gels of purifications from *Drosophila* S2 cells expressing RacGAP50C::PrA or Pav-KLP::PrA. The positions of some proteins identified by MS are indicated on the right. (B) Silver-stained gel of Nesd::PrA purification. Bands corresponding to Pav-KLP and RacGAP50C are indicated. The table shows the relative MS score and number of peptides of the top five MS hits. The bait Nesd is indicated in red. The numbers on the left indicate the sizes in kilodaltons of the molecular mass markers. (C) GST::Nesd purified from bacteria was incubated with either RacGAP50C$_{1–371}$ or Pav-KLP$_{461–887}$, translated, and radiolabeled in vitro and then pulled down using glutathione beads. The colloidal Coomassie blue (CCB) staining of the protein loading is shown at the bottom. On the right is a schematic summary of the positive (+) and negative (−) results of the GST pull-down assays using different RacGAP50C and Pav-KLP fragments. C1, phorbol ester/diacylglycerol binding; Pbl, Pebble; Ani, Anillin; Kinesin, kinesin catalytic domain; CC, coiled coil; RacGAP, RacGAP50C.

parallel β strands, was originally described in enzymes secreted by bacterial plant pathogens to digest the sugars present on the plant cell wall and then found in a variety of proteins that display affinity for carbohydrates (Mayans et al., 1997). In an initial attempt to characterize the functions of these two domains, we tested the ability of different Nesd fragments to localize to the midbody and interact with centralspindlin (Fig. 2, E–G). All fragments containing NHD localized to the midbody and interacted with PrA-tagged RacGAP50C in S2 cells, whereas the PLD motif showed diffuse cytoplasmic localization and was not necessary for binding to RacGAP50C (Fig. 2, E–G). Similar results were obtained using the other centralspindlin component Pav-KLP (Fig. S2 A). These observations suggest that Nesd binds to the centralspindlin complex via its conserved NHD motif and that this interaction is necessary for Nesd localization to the midbody. We could not test, however, whether centralspindlin was directly required for Nesd localization to the midbody in S2 cultured cells or fly tissues because inactivation of either component of the complex by RNAi or mutation prevents furrowing (Adams et al., 1998; Somma et al., 2002; Goshima and Vale, 2003; Somers and Saint, 2003). In contrast, we found that RNAi depletion of Nesd did not cause any obvious cytokinesis or cell division defects. Moreover, both centralspindlin subunits and the CR component Anillin accumulated properly in *nesd* RNAi cells (Fig. S2 B and not depicted), indicating that Nesd is not essential for cytokinesis in S2 cells.

Nesd displays binding affinity for β-galactosides in vitro

The presence of a PLD domain suggested that Nesd could bind to poly- or oligosaccharides (Mayans et al., 1997). To assess Nesd affinity for specific glycans, we screened an array of >300 different glycans in collaboration with the Consortium for Functional Glycomics (CFG) using a recombinant His-tagged Nesd protein. Two separate experiments indicated that Nesd had high binding affinity in vitro for β-galactosides (a full list of data is available at the CFG website; Fig. 3), including galactose β1–3 *N*-acetylgalactosamine (Galβ1–3GalNAc), the major

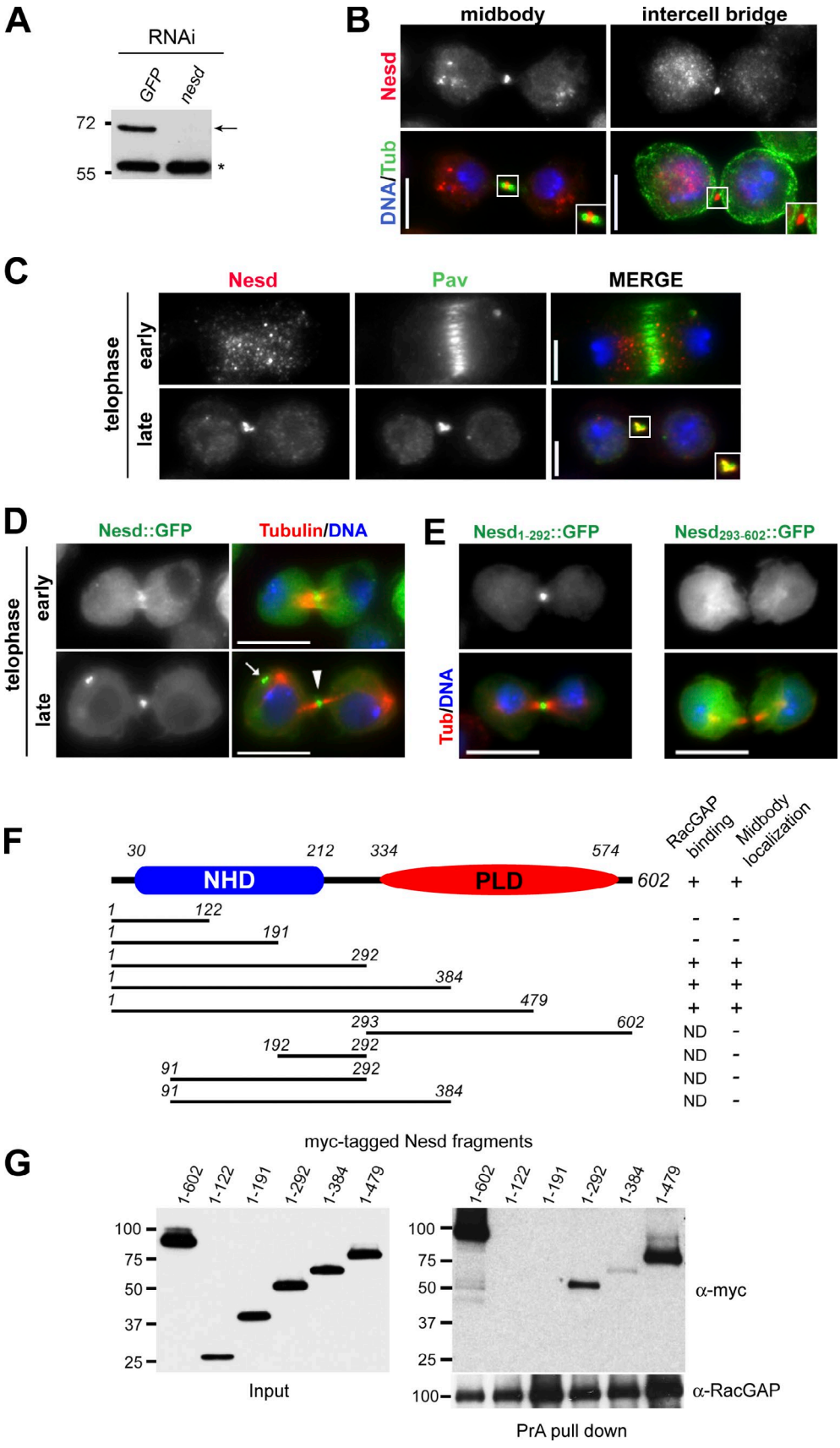

Figure 2. **The Nesd N-terminal domain is required for midbody localization and interaction with centralspindlin.** (A) Western blot analysis of Nesd protein levels in *Drosophila* S2 cells treated for 72 h with either *GFP* (control) or *nesd* dsRNA. The arrow marks the band corresponding to the Nesd protein, whereas the asterisk marks a nonspecific band used as a loading control. (B) *Drosophila* S2 cells were fixed and stained to detect Nesd, tubulin (Tub), and DNA.

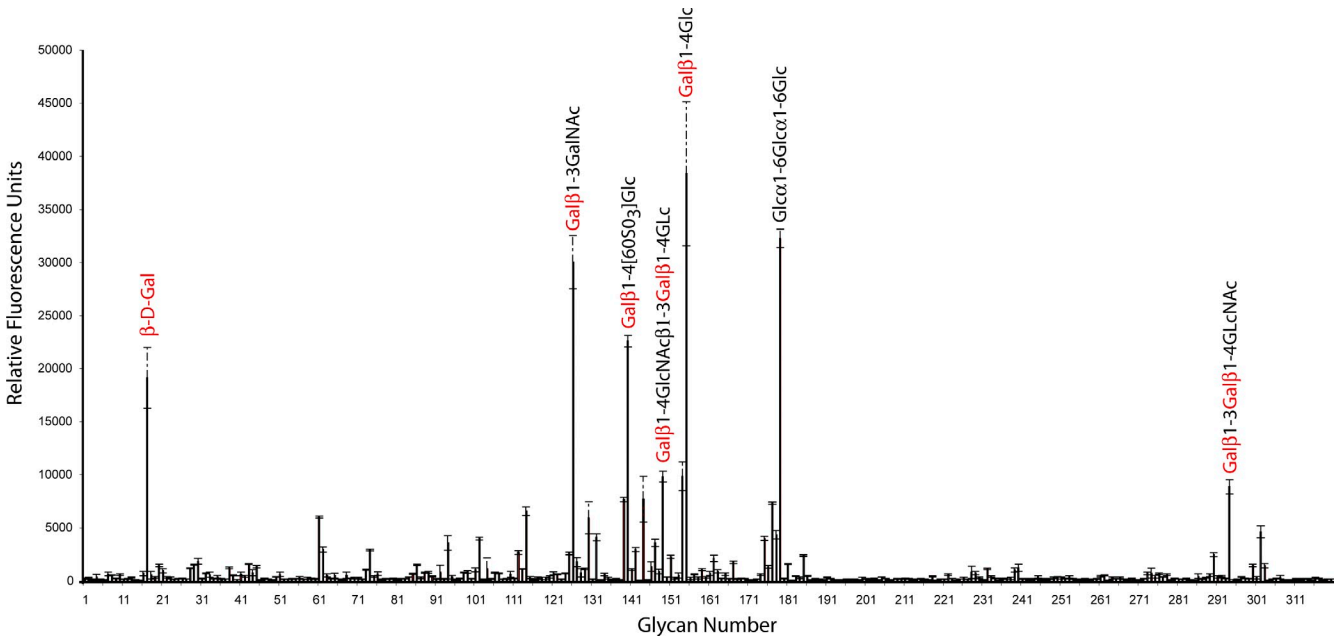

Figure 3. **A glycan array screen revealed Nesd affinity for β-galactosides.** His-tagged Nesd was expressed in a baculovirus system and used to screen an array of 320 glycans (version 3.0) spotted in six replicates. Nesd binding was detected first using an anti-His rabbit antibody and then an anti–rabbit IgG Alexa Fluor 488. The experiment was replicated twice with very similar results, and complete sets of data are available at the CFG website. The graph here shows the results of one of these experiments in which each glycan was plotted against its mean relative fluorescence intensity. The top high affinity ligands are indicated on the chart, and β-galactose residues are highlighted in red. The error bars indicate standard deviations.

O-glycan identified in a survey of the *Drosophila* glycome (North et al., 2006). This evidence suggests that Nesd could interact with O-glycosylated proteins in vivo.

Nesd properties are conserved in human cells

A Position-Specific Iterated Basic Local Alignment Search Tool (PSI-BLAST) search found Nesd orthologues in insects, marine invertebrates, and vertebrates, including all sequenced mammalian species, but not in *Caenorhabditis elegans* and yeasts (Fig. 4, A and B; and not depicted). This analysis allowed us to build the protein evolutionary tree, which fits the known species tree (Fig. 4 B). The Nesd general structure with an NHD domain in the N terminus and a PLD domain in the C terminus is well conserved in many of these orthologues, and, as mentioned before, the highest homology was always found in the NHD region. The closest human orthologue, which shows a 27% identity with the NHD region of *Drosophila* Nesd (23% over the entire length of the protein; Fig. 4 A), was a protein dubbed Shc SH2 domain–binding protein 1 (SHCBP1) because its mouse homologue (also known as mPAL) was found to interact in a yeast two-hybrid system with the SH2 domain of the Shc adaptor protein (Schmandt et al., 1999). Despite the significant conservation, we never identified the *Drosophila* Shc homologue in our numerous Nesd affinity purifications, and, therefore, it is unclear whether this interaction occurs in flies.

To test whether Nesd properties had been conserved in humans, we first analyzed the localization of GFP-tagged SHCBP1 in both HeLa and U2OS cells. SHCBP1::GFP displayed a weak localization to the spindle midzone in some early telophase cells but was always found to concentrate at the midbody in late cytokinesis (Fig. 5 A), where it colocalized with both human centralspindlin components RacGAP1 and MKLP1 (Fig. 5 B and not depicted). Immunoprecipitation experiments showed that SHCBP1::GFP could also pull down both RacGAP1 and MKLP1, confirming that this interaction is conserved in humans (Fig. 5 C). However, RNAi depletion of SHCBP1 in either HeLa or U2OS cells showed no increase in multinucleate cells (Fig. S3), which was similar to the results obtained in *Drosophila* cultured cells. Finally, because MKLP1 depletion in human cells does not

(C) *Drosophila* S2 cells were fixed and stained to detect Nesd, Pav-KLP (Pav), and DNA (blue in the merged image). The punctate staining in the red channel of the early telophase cell is not specific because it is not eliminated after *nesd* RNAi (Fig. S1 B). Bars, 5 µm. (B and C) Insets show magnifications of the midbody. (D) *Drosophila* S2 cells stably expressing Nesd::GFP were fixed and stained to detect GFP, tubulin, and DNA. The arrowhead marks Nesd localization to the midbody ring, whereas the arrow indicates a midbody remnant. (E) *Drosophila* cells stably expressing two Nesd fragments (1–292 and 293–602) tagged with GFP were fixed and stained to detect GFP, tubulin, and DNA. (B, D, and E) Bars, 10 µm. (F) Schematic representation of the midbody localization and interaction with RacGAP50C of several Nesd fragments. The positions of the NHD and PLD are indicated. Nesd fragments were tagged at either the N or C terminus with GFP, and their localizations were then analyzed in S2 cells. C-terminal myc-tagged Nesd fragments were used to test the interaction with RacGAP50C. (G) *Drosophila* S2 cells stably expressing RacGAP::PrA were transfected with the indicated myc-tagged Nesd fragments, and protein extracts were analyzed by Western blotting using an anti-myc (α-myc) antibody (input). The same extracts were then subject to PrA pull-down assay, and the presence of myc-tagged fragments in the pull-down was detected by Western blotting. The numbers on the left indicate the sizes in kilodaltons of the molecular mass markers.

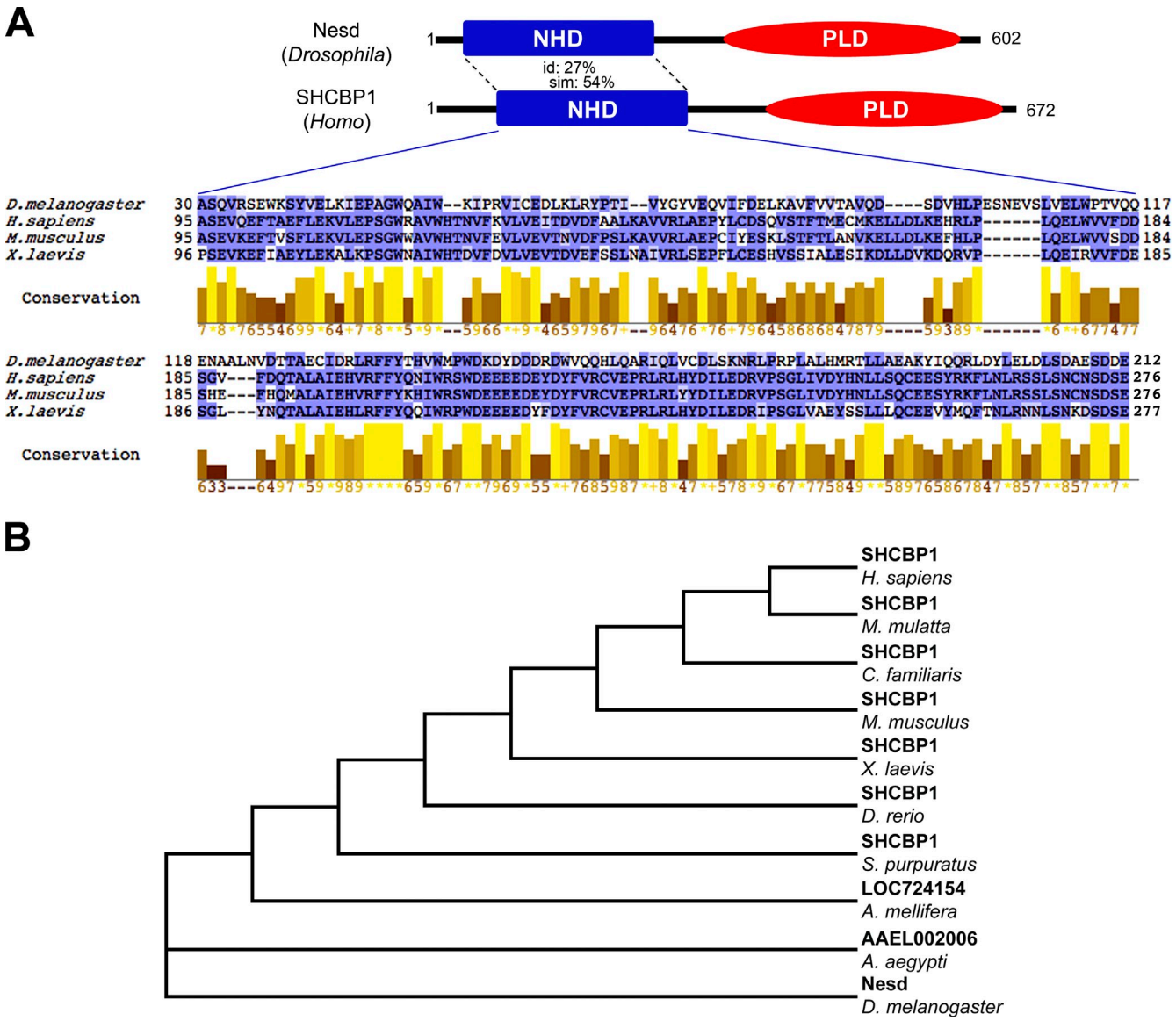

Figure 4. **Nesd is an evolutionarily conserved protein.** (A) At the top is a schematic alignment of *Drosophila* Nesd and its human counterpart SHCBP1. The Nesd homology domain (NHD) and pectin lyase–like domain (PLD) are indicated. The percentages of identities (id: 27%) and positives (similarity, sim: 54%) found in the NHD regions of the two orthologues are also indicated. An alignment of the NHD found in *Drosophila*, human, mouse, and frog is shown at the bottom using the Blosum62 coloring scheme (matches are highlighted in dark blue, and positive alignment scores are highlighted in light blue). The domain shows high conservation throughout the four species, as depicted by the conservation histogram below the alignment (yellow and brown bars); numerical indices and gradual shading reflect the conservation of physicochemical properties in the alignment, with identities scoring highest and indicated by asterisks. (B) Unrooted phylogenetic tree of the Nesd orthologues in 10 species spanning vertebrates, insects, and echinoderms. The tree, which shows the evolutionary relations between the proteins, is consistent with the corresponding species tree.

always prevent furrowing (Matuliene and Kuriyama, 2002), we tested whether centralspindlin was required for SHCBP1 localization to the midbody. About 55% of the MKLP1-depleted cells (n = 100) that completed furrow ingression did not show any accumulation of SHCBP1 at the cleavage site (Fig. 5 D). In the remaining 45%, SHCBP1::GFP staining was very weak and diffuse along CS microtubules (Fig. 5 D). These results suggest that MKLP1 is necessary for proper localization of SHCBP1 during cytokinesis, although this could be an indirect effect because midbody formation is impaired after MKLP1 depletion (Matuliene and Kuriyama, 2002). In conclusion, our data indicate that Nesd structure, localization, and interaction with centralspindlin are conserved in humans.

nesd is essential for viability and cytokinesis during male meiosis

The lack of cytokinesis failure after *nesd* RNAi in fly and human cultured cells prompted us to investigate whether *nesd* was instead essential in the fly. We found that flies containing a transposable *P*-element insertion 53 nt upstream of the ATG starting codon (hereafter dubbed $nesd^1$) were homozygous viable, but males were semisterile (see following paragraph). Flies harboring $nesd^1$ over a deficiency that completely uncovers the *nesd* genomic region, *Df(2L)ED1305*, were semilethal (Fig. 6 A), indicating that $nesd^1$ is a hypomorphic allele. This lethality could be rescued by precise excision of the *P* element and by expression of a *nesd::GFP* transgene expressed under a ubiquitous

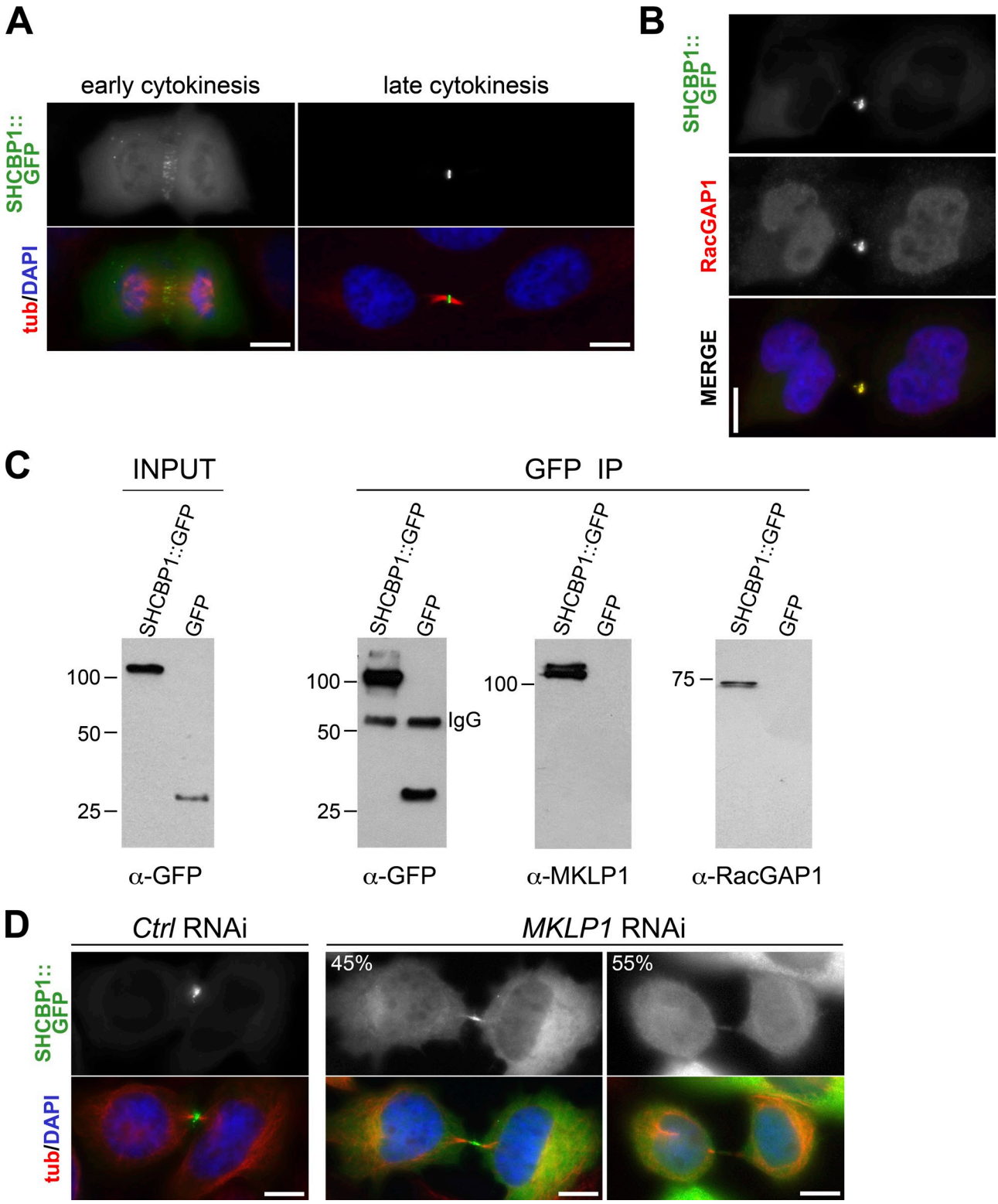

Figure 5. **The human Nesd counterpart localizes to the cleavage site and interacts with centralspindlin.** (A) HeLa cells were transiently transfected with a construct expressing SHCBP1::GFP and, after 48 h, fixed and stained to detect GFP, tubulin (tub), and DNA (blue in the merged image). (B) HeLa cells were transiently transfected with a construct expressing SHCBP1::GFP and, after 48 h, fixed and stained to detect GFP, RacGAP1, and DNA (blue in the merged image). (C) Extracts from HeLa cells transiently expressing either GFP or SHCBP1::GFP were immunoprecipitated using GFP antibodies (GFP IP). The Western blot on the left (INPUT) shows the level of expression of the GFP proteins. The presence of the two centralspindlin components MKLP1 and RacGAP1 in the SHCBP1::GFP pull-downs was confirmed by Western blotting. The position of IgG bands is indicated. The numbers on the left indicate the sizes in kilodaltons of the molecular mass markers. (D) HeLa cells transiently expressing SHCBP1::GFP were transfected with either control scramble or MKLP1 siRNAs for 48 h and then fixed and stained to detect GFP, tubulin, and DNA (blue in the merged image). The percentage of cells without any accumulation of SHCBP1 at the cleavage site (55%) or very weak and diffuse SHCBP1::GFP staining along CS microtubules (45%) is indicated. Bars, 10 µm.

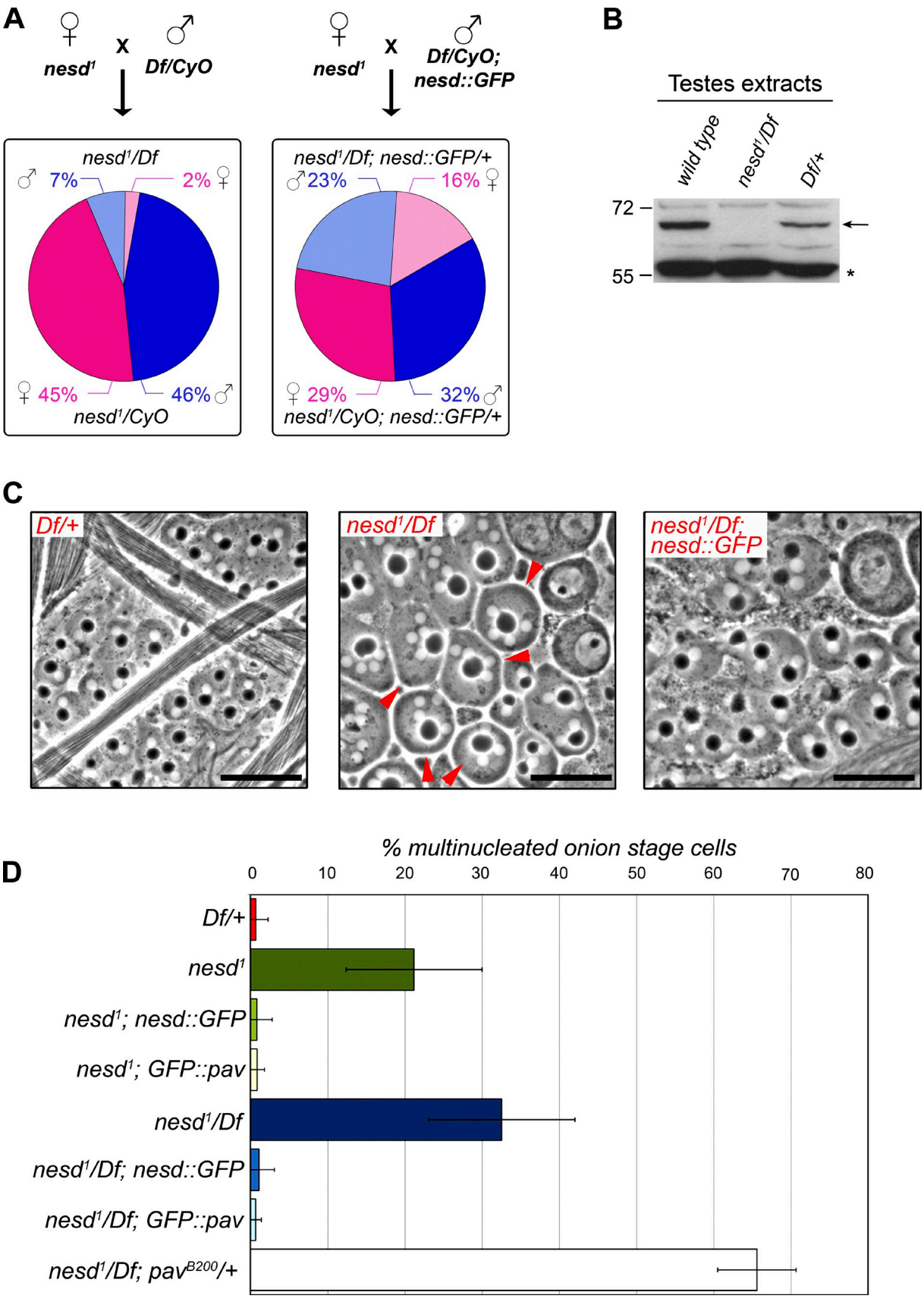

Figure 6. **Nesd is required for viability and spermatocyte cytokinesis.** (A) Analysis of the lethality of *nesd*[1] mutants. Homozygous *nesd*[1] females were crossed to either *Df(2L)ED1305/CyO* (*Df/CyO*) or *Df(2L)ED1305/CyO;nesd::GFP* (*Df/CyO;nesd::GFP*) males, and the resulting progeny is indicated in the left and right pie charts, respectively. The male and female progenies are indicated in light/dark blue and light/dark pink, respectively. At least 400

promoter (Fig. 6 A and not depicted), confirming that the *P*-element insertion present in *nesd*^{1} flies was directly responsible for the mortality.

To gain insights into potential functions of *nesd* during cell division, we decided to analyze cytokinesis during the two male meiotic divisions because previous studies indicated that several genes that are required for cytokinesis during male meiosis are not always essential for mitosis (Giansanti et al., 2001, 2004). Western blot analysis indicated that Nesd is expressed in testes and is virtually undetectable in *nesd*^{1}/*Df(2L)ED1305* hemizygous pharate adults, providing a molecular confirmation that this mutant is a severe hypomorph (Fig. 6 B). The final products of the two male meiotic divisions are round, so-called "onion-stage," spermatids containing a single phase-lucent nucleus paired with a single, similarly sized phase-dense mitochondrial derivative, the Nebenkern (Fig. 6 C). Control onion-stage spermatids contained a 1:1 ratio of haploid nuclei/Nebenkerns of similar size (Fig. 6, C and D). In contrast, *nesd*^{1} homozygous and *nesd*^{1}/*Df(2L)ED1305* hemizygous mutant flies exhibit multinucleate spermatids in 21.2 and 32.5% of the cells, respectively (Fig. 6 D). These spermatids contained either two of four haploid nuclei accompanied by an enlarged Nebenkern (Fig. 6 C). This is a clear indication of cytokinesis failure during one or both meiotic divisions. Consistent with this cytokinesis failure, ∼50% of *nesd*^{1} homozygous males and 80% of *nesd*^{1}/*Df(2L)ED1305* hemizygous males were sterile. Finally, both precise excision of the *P* element present in *nesd*^{1} flies and expression of a *nesd::GFP* transgene could rescue the cytokinesis defects of *nesd* mutants (Fig. 6 D and not depicted), confirming that this phenotype was the direct result of a lesion in the *nesd* gene. However, a *nesd* transgene containing the GFP tag at the N terminus was unable to rescue both the lethality and the cytokinesis defects of *nesd*^{1} mutants, even though it localized like its C-tagged counterpart. Six out of eight *GFP::nesd* lines showed a modest, but significant, increase of multinucleate onion-stage spermatids (>5%; unpublished data). These results suggest that the addition of the GFP tag to the Nesd N terminus might interfere with its functions and probably generates a dominant-negative mutant. Finally, three different transgenic strains carrying the NHD alone ($Nesd_{1–292}$) tagged with GFP at either the N or C terminus could not rescue the lethality and cytokinesis defects of *nesd* mutants, even though the transgenes were expressed at significant levels (Fig. S4 A). These findings indicate that the PLD is necessary for Nesd function. In conclusion, our results demonstrate that *nesd* is an essential gene in the fly and is also required for cytokinesis during male meiosis.

nesd is required for completion of cytokinesis during male meiosis

To characterize in detail the cytokinesis defects in *nesd* mutants, we observed live spermatocytes undergoing the first meiotic division by multidimensional differential interference contrast (DIC) and fluorescence time-lapse microscopy (Inoue et al., 2004). To visualize the cell cortex and the assembly and constriction of the actomyosin ring, we used the myosin regulatory light chain encoded by the *spaghetti squash* (*sqh*) gene tagged with GFP (Royou et al., 2004). In this way, we could directly observe chromosome dynamics in the DIC images and furrow ingression by GFP fluorescence. In both control and *nesd*^{1} mutant spermatocytes, CR assembly and constriction started 5 min after the chromosomes reached the poles (Fig. 7 A and Videos 1 and 2). The rate of furrow ingression was similar in control and *nesd* mutants (Fig. 7 B), but whereas CR constriction was symmetric in the majority of control cells (83.6%, $n = 45$), the CR constricted asymmetrically in 46.5% ($n = 63$) of *nesd*^{1} spermatocytes (Fig. 7 A, 20, 25, and 30 min). Subsequently, the cleavage furrow collapsed (Fig. 7 A, 35 min), a phenotype never observed in wild-type controls. Sqh::GFP initially accumulated at the cleavage furrow in *nesd* spermatocytes (Fig. 7 A, 20 and 25 min), but the signal became very weak at late stages, and the CR failed to form a robust circular structure (Fig. 7 A, 30, 35, and 45 min). At the same time, membrane invagination collapsed, and isolated CR remnants could be observed in the cytoplasm (Fig. 7 A, arrowheads).

Sqh::GFP marked the cell cortex underlying the plasma membrane but not the membrane itself. Therefore, to confirm our results, we directly visualized membrane invagination in live spermatocytes using the pleckstrin homology (PH) domain of PLCδ tagged with GFP (Wong et al., 2005). These experiments confirmed that cytokinesis failed in 49% ($n = 56$) of *nesd* spermatocytes, and plasma membrane invagination was asymmetric and incomplete in 27% of these cells compared with the normal symmetric invagination observed in the vast majority (90%, $n = 39$) of controls (Fig. 7 C). Together, these results indicate that, unlike its centralspindlin partner, Nesd is not essential for furrow ingression but rather for CR stability and the attachment of the furrowing membrane to the actomyosin ring in late telophase.

Ring canal formation is compromised in *nesd* female and male germline cells

Our time-lapse analyses indicated that cytokinesis in *nesd* spermatocytes failed after furrow ingression but before the formation of ring canals. To analyze ring canal formation in *nesd* mutants, we first attempted to follow the dynamics of GFP-tagged

animals per each cross were counted. (B) Western blot analysis of Nesd protein levels in testes dissected from wild-type, *nesd*^{1}/*Df(2L)ED1305* (*nesd*^{1}/*Df*), and *Df(2L)ED1305/+* (*Df/+*) adult males. The arrow indicates the band correspondent to Nesd protein, whereas the asterisk marks a nonspecific band used as a loading control. (C) Phase-contrast micrographs of onion-stage spermatids dissected from *Df(2L)ED1305/+* (control), *nesd*^{1}/*Df(2L)ED1305*, and *nesd*^{1}/*Df(2L)ED1305;nesd::GFP* (*nesd*^{1}/*Df;nesd::GFP*) males. Multiple white nuclei associated with a large dark Nebenkern were observed in *nesd*^{1}/*Df(2L)ED1305* hemizygous mutants (arrowheads). Bars, 50 µm. (D) Quantification of the number of multinucleate spermatids observed in testes dissected from flies of the genotypes described in C and also from *nesd* homo- (*nesd*^{1}) and hemizygous (*nesd*^{1}/*Df(2L)ED1305*) mutants carrying either a GFP::Pav-KLP transgene (*GFP::Pav*) or the *pav*^{B200} allele. More than 700 onion-stage spermatids per genotype were counted in three separate experiments; the error bars indicate standard deviations.

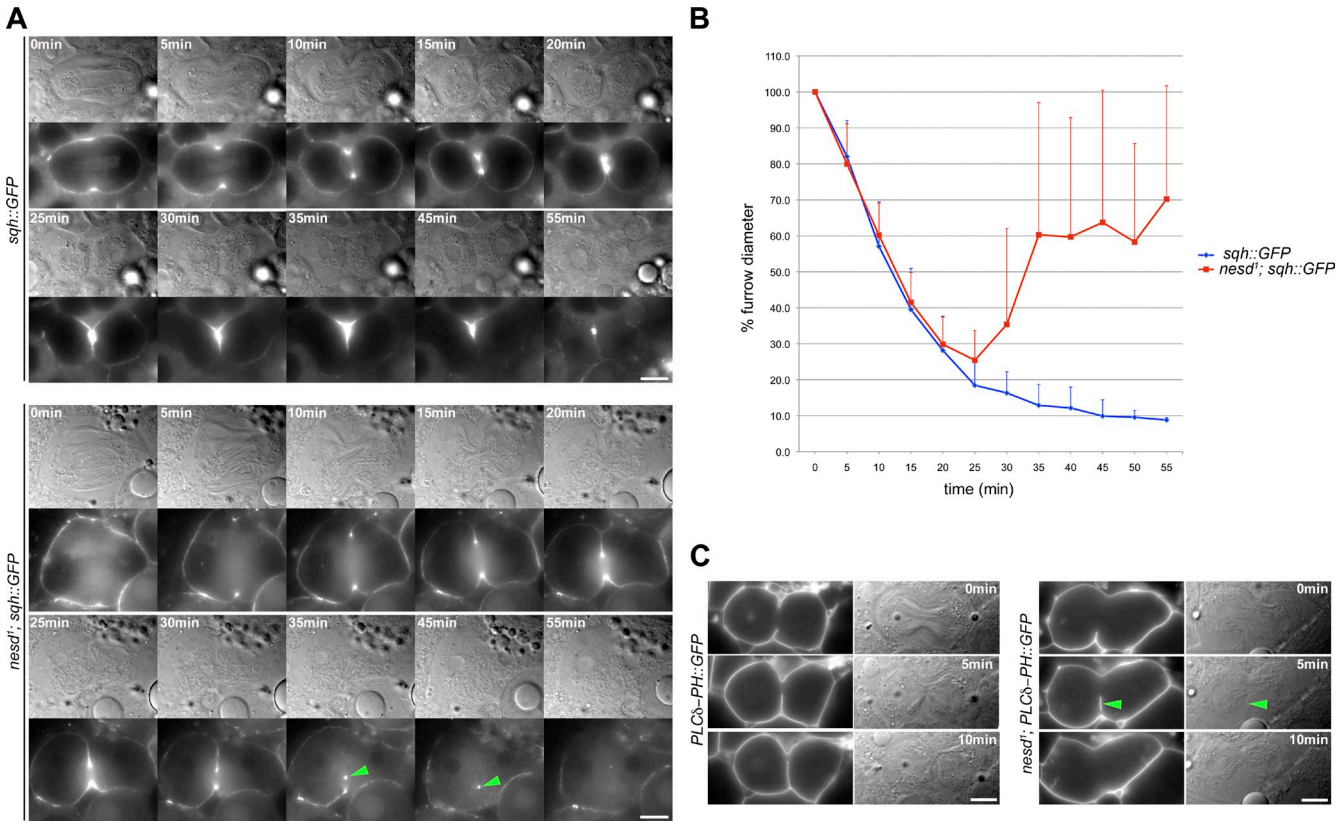

Figure 7. ***nesd* mutant spermatocytes show late cytokinesis failure.** (A) Selected frames from time-lapse sequences of live spermatocytes expressing an *sqh::GFP* transgene in either a wild-type (*sqh::GFP*) or *nesd*^{1} (*nesd*^{1}*;sqh::GFP*) mutant background. DIC images are shown at the top, and the relative fluorescence images are shown at the bottom. The arrowheads indicate the CR after furrow collapse. Time relative to the end of anaphase (when chromosomes reached the poles) is indicated at the top. (B) Furrow ingression dynamics during cytokinesis in wild-type (*sqh::GFP*) and *nesd*^{1} (*nesd*^{1}*;sqh::GFP*) spermatocytes plotted over time. Furrow diameters were measured from eight wild-type and 10 *nesd* mutants (including the cells shown in Fig. 7 A). The error bars indicate standard deviations. (C) Images of live spermatocytes expressing a *PLCδ-PH::GFP* transgene in either a wild-type (*PLCδ-PH::GFP*) or *nesd*^{1} (*nesd*^{1}*;PLCδ-PH::GFP*) mutant background. DIC images are shown on the right, and relative fluorescence images are shown on the left. The arrowheads indicate the invaginating membranes. Bars, 10 µm.

Pav-KLP, a key ring canal component, in live *nesd* spermatocytes. However, we found that overexpression of the GFP::Pav-KLP transgene fully rescued the cytokinesis defects and sterility, but not the lethality, of *nesd* mutants (Fig. 6 D and not depicted). Consistent with this result, normal cytokinesis figures were observed in *nesd*^{1}*/Df;GFP::pav* spermatocytes (Fig. S4 B). In addition, *nesd*^{1}*/Df* hemizygous mutants carrying a single copy of the *pav*^{B200} allele (Adams et al., 1998) showed a twofold increase of multinucleate spermatids (Fig. 6 D). These genetic interactions reflect the strong binding affinity of these two proteins and indicate that extra Pav-KLP can compensate for the reduction of Nesd during spermatocyte cytokinesis, whereas a reduction of Pav-KLP enhances the cytokinesis defects of *nesd* mutants. Moreover, it also suggests that Nesd must have some additional functions besides its role in spermatocyte cytokinesis, which are independent of its interaction with Pav-KLP, because GFP::Pav could not rescue *nesd* lethality.

As an alternative approach to live imaging of GFP::Pav-KLP, we immunostained *nesd* mutant spermatocytes for Pav-KLP and another ring canal component, Anillin. In both cases, we found that both proteins localized normally in early telophase in these mutants (Fig. S4 C and not depicted) but failed to assemble into a ring-shaped structure in late cytokinesis (Fig. 8, A and B, arrowheads). Interestingly, normal ring canals were found to interconnect the gonial cells formed during the four mitotic divisions that preceded meiosis I (Fig. 8 B, arrows; and not depicted), indicating that ring canals failed to assemble only during late cytokinesis in male meiosis. Moreover, microtubule staining confirmed that CR constriction occurred asymmetrically in *nesd* mutant spermatocytes because the CS was displaced to the side of the cell (Fig. 8 A).

These results prompted us to examine in detail the formation of ring canals during oogenesis in *nesd* mutants, even though sterility was not observed in *nesd* adult females. Actin staining revealed that a significant number (38%, $n = 39$) of *nesd* egg chambers at stage 9 or 10 contained remnants of ring canals associated with binucleate nurse cells (Fig. 8 C, arrows). These defects were never observed in control animals or *nesd* egg chambers from an earlier developmental stage, suggesting that *nesd* is also required to stabilize ring canals at late stages during oogenesis.

We tried to examine the localization of Nesd in both male and female germ cells. Unfortunately, our antibody was unable to detect Nesd in fixed preparations of testes or ovaries, even though a clear signal was observed in Western blot experiments (Fig. 6 B and not depicted). To overcome this problem, we analyzed the localization of a Nesd::GFP transgene expressed under

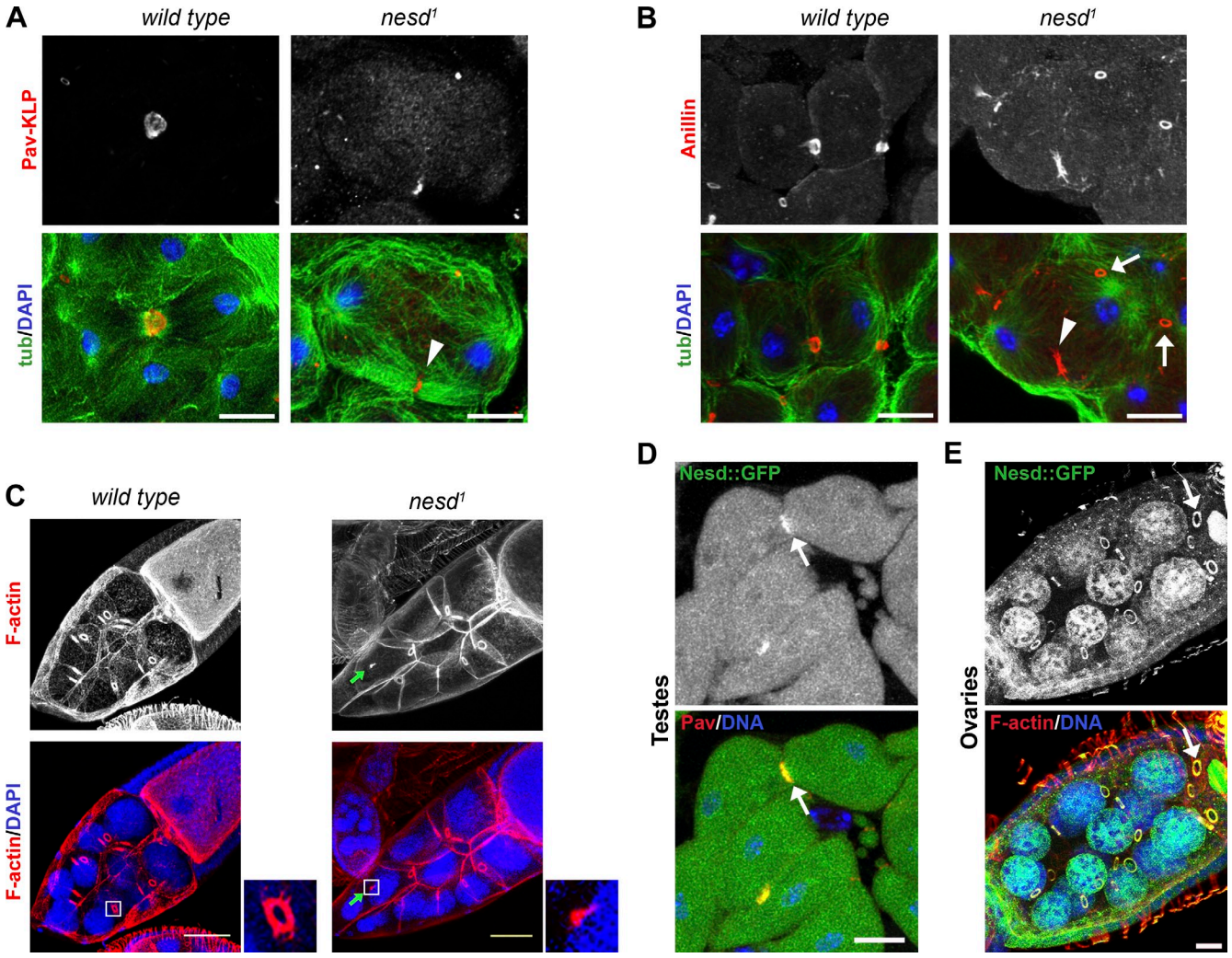

Figure 8. **The formation of ring canals is compromised in *nesd* male and female germline cells.** (A) Testes dissected from either *wild-type* or *nesd*^{1} homozygous male pupae were fixed and stained to detect Pav-KLP, tubulin (tub), and DNA (blue in the merged image). The arrowhead indicates a remnant of a ring canal in the *nesd*^{1} spermatocyte. (B) Testes dissected from either *wild-type* or *nesd*^{1} homozygous male pupae were fixed and stained to detect Anillin, tubulin, and DNA. The arrowhead indicates an abnormal CR in the *nesd*^{1} spermatocyte. The ring canals marked by the arrows were probably generated during the four spermatogonial mitoses as judged by their position in the cyst. (C) Stage 10 egg chambers from *wild-type* and *nesd*^{1} ovaries stained for F-actin and DNA. The arrows mark an aberrant ring canal in a binucleate nurse cell. Magnifications are shown in the insets. (D) Testes expressing a *nesd::GFP* transgene were fixed and stained to detect GFP, Pav-KLP, and DNA. (A, B, and D) Bars, 10 µm. (E) Stage 9 egg chamber dissected from flies expressing a *nesd::GFP* transgene and fixed and stained to detect GFP, F-actin, and DNA. (D and E) The arrows indicate ring canals. (C and E) Bars, 50 µm.

a ubiquitous promoter in male and female germ cells. Nesd::GFP clearly accumulated at ring canals in testes and ovaries at all stages, where it colocalized with Pav-KLP and F-actin, respectively (Figs. 8, D and E; and S5 A; and not depicted). Time-lapse analysis in primary spermatocytes also confirmed that Nesd::GFP accumulated at ring canals after CR constriction (Video 3), although a faint signal could also be observed in fixed preparations earlier during cytokinesis (not depicted), which was consistent with our findings in cultured cells (Fig. 2 D). A weak Nesd::GFP signal could also be observed at the fusome, a branched cytoplasmic structure that connects all mitotic cells in a germ cell syncytium, in testes but not in ovaries (Fig. S5, A and B).

Although ring canals in male and female germline cells are functionally equivalent, they have slightly different compositions. In addition to centralspindlin and Anillin, female ring canals contain actin and the cytoskeletal proteins hu-li tai shao (Hts) and Kelch, which are deposited to form an inner rim after the four mitotic divisions of the cystoblast (Yue and Spradling, 1992; Xue and Cooley, 1993; Tilney et al., 1996). Costaining with Hts in stage 4 egg chambers indicated that Nesd::GFP localized to the outer rim of female ring canals (Fig. S5 C) like its partner Pav-KLP (Minestrini et al., 2002). Consistent with this, Nesd could be detected at ring canals early during oogenesis, in region 1 of the germarium where the first four mitotic divisions of the cystoblast occur (Fig. S5 B). We conclude that Nesd is a novel component of ring canals in both female and male germline cells.

Discussion

Nesd is a novel centralspindlin partner required for spermatocyte cytokinesis

Our results identified Nesd as a new, evolutionarily conserved partner of the centralspindlin complex. Unlike the other centralspindlin-interacting proteins identified so far, Nesd can directly

bind to both Pav-KLP and RacGAP50C. This interaction requires a highly conserved region in the Nesd N terminus, which also mediates its localization to the midbody ring during cytokinesis in cultured cells. This suggests that centralspindlin is necessary for Nesd recruitment to the midbody, and in support of this hypothesis, the human orthologue SHCBP1 fails to properly localize in MKLP1-depleted cells.

Nesd is necessary for cytokinesis in spermatocytes and possibly female germ cells, but not in cultured cells, during spermatogonial divisions and in somatic cells, such as neuroblasts (unpublished data). This is not surprising because a previous study has identified several genes that are required for cytokinesis in *Drosophila* male meiosis but are dispensable for mitosis (Giansanti et al., 2004). However, it is important to point out that Nesd does not have a meiosis-specific function because it is also required for ring canal formation during the mitoses that lead to the development of female germline cysts. Thus, we propose that Nesd might be essential for cytokinesis only in specific cell types, such as large spermatocytes and nurse cells.

Our time-lapse analyses indicated that furrows ingressed almost completely, although asymmetrically, in *nesd* spermatocytes, but CRs became unstable in late cytokinesis, and furrows subsequently collapsed. Thus, Nesd is not essential for furrow ingression but is required for stabilization of the actomyosin ring in late cytokinesis and to maintain the association of the plasma membrane with the CR. Consistent with these phenotypes, Nesd does not strongly accumulate at the CS midzone in early telophase like centralspindlin, but it is instead recruited to the midbody ring or ring canals in late telophase. This localization pattern and the presence of abnormal ring canals in both *nesd* mutant spermatocytes and egg chambers suggest that Nesd might be required for the stability of the CR in late cytokinesis and its conversion into a ring canal. That Nesd could function as a scaffold protein required for CR stability and ring canal formation might also explain the genetic interaction between *nesd* and *pav*. If Nesd does indeed function to stabilize centralspindlin during cytokinesis, its absence could be compensated by the presence of additional Pav-KLP, and reduced levels of this kinesin would exacerbate *nesd* cytokinesis defects.

Nesd::GFP also localized weakly to fusomes in male, but not female, germline cysts. Fusomes are cytoplasmic organelles necessary for the development of male and female germ cell cysts; they break down and disappear after cyst formation in the ovary but persist throughout sperm development (de Cuevas et al., 1997). We never observed a defect in the development of male or female germline cysts, and Nesd::GFP does not accumulate at the fusome in spermatocytes. Therefore, Nesd localization to the fusome does not seem to reflect a specific function in the development and/or synchronization of germ cell cysts. However, our $nesd^{1}$ allele is not null, and, therefore, it is also possible that the low levels of Nesd present in our mutant or the maternal contribution of this protein might be sufficient for the development of male germ cells.

Nesd shows strong affinity for both centralspindlin components in vivo and in vitro, but it colocalizes with centralspindlin only in late cytokinesis. Thus, we surmise that either some posttranslational modifications (e.g., phosphorylation and/or glycosylation) or the interaction with other factors prevents Nesd association with centralspindlin in early telophase. Interestingly, it has been recently proposed that the interaction of MKLP1 with 14-3-3 proteins is transiently inhibited during furrow ingression by Aurora B phosphorylation to allow a stable association of this kinesin with the CS midzone (Douglas et al., 2010). This phosphorylation would then be reversed at the end of cytokinesis when Aurora B is inactivated, allowing MKLP1 and 14-3-3 to associate during midbody formation. A similar mechanism could also regulate the interaction between centralspindlin and Nesd, as 14-3-3 proteins were also identified in our Nesd::PrA affinity purifications (Fig. 1 B). Thus, Nesd may interact with centralspindlin when it is associated with 14-3-3. Consistent with this hypothesis, 14-3-3 proteins localize to ovarian ring canals (Benton et al., 2002).

It is not known whether the Nesd mammalian orthologues SHCBP1 or mPAL accumulate at intercellular bridges. However, this is a possibility given that SHCBP1 localizes to the midbody and interacts with centralspindlin in human cells. Moreover, both centralspindlin components were identified in a proteomic survey of proteins enriched at the intercellular bridges of male mice, and MKLP1 was also found to interact with the testis-expressed gene 14 protein (TEX14; Greenbaum et al., 2007), a mouse intercellular bridge component necessary for the establishment of ring canals in male and female germ cells.

Nesd highlights the importance of glycosylation in late cytokinesis

Nesd contains a PLD, and our in vitro binding assay experiments suggest that it could bind to O-glycosylated proteins in vivo. Unfortunately, no established technique is currently available to analyze the interaction of proteins with glycans in vivo, and, thus, we were unable to confirm that Nesd interacts with carbohydrates in cultured cells or spermatocytes. A role for glycosylation during cytokinesis has been documented in *C. elegans*, *Drosophila*, and mammalian cells (Slawson et al., 2005; Wang et al., 2005; Zhang and Ten Hagen, 2010), and a recent study indicated that cross talk between glycosylation and phosphorylation could regulate cytokinesis in human cells (Wang et al., 2010). Our findings suggest that glycosylated proteins could also be important for late cytokinesis in the *Drosophila* germline. Consistent with our results, an enrichment of glycosylated proteins at *Drosophila* ring canals was proposed >40 yr ago (Koch and King, 1969), and a mucinlike glycoprotein, mucin D, was found to be one of the first components recruited to ring canals in ovaries and in male pre- and postmeiotic cysts (Kramerova and Kramerov, 1999). Coincidently, the O-linked carbohydrate component of mucin D consists mainly of Galβ1-3GalNAc disaccharides (Kramerov et al., 1996), which was one of the top hits identified in our glycan screen. Thus, Nesd could provide a link between glycosylated proteins and centralspindlin during the initial assembly of ring canals in both male and female germ cells. Unfortunately, the primary amino acid sequence of mucin D is not known, and, therefore, we cannot establish whether it was identified in our Nesd::PrA purifications. It is important to point out, however, that Nesd does not have a transmembrane domain or a secretion signal sequence,

suggesting that most likely it cannot cross the plasma membrane and, therefore, should not be able to interact with glycoproteins and proteoglycans located on the external surface of the cell. However, there is increasing evidence that glycosylated proteins can be found in the cytoplasm (Hart et al., 2007; Wang et al., 2010), and it will be interesting in the future to characterize the glycosylation profiles of ring canal components to assess whether these oligosaccharides can interact with Nesd.

Materials and methods

Cell culture, DNA transfection, and RNAi treatments

The Dmel strain of S2 cells (Invitrogen) was grown in serum-free medium supplemented with antibiotics. Double-stranded RNA (dsRNA) production and RNAi treatments were performed as described previously (D'Avino et al., 2006). Generation of blasticidin-resistant stable cell lines was performed as previously described (D'Avino et al., 2009), with the only exception that transfection reagent (FuGENE HD; Roche) was used according to the manufacturer's instructions. Human HeLa and U2OS cells were maintained in DME (Invitrogen) supplemented with 10% FCS and antibiotics. siRNAs were designed and purchased from the MWG Operon (Eurofins). DNA and siRNA transfections were performed as described previously (Montembault et al., 2007).

Molecular biology

Gateway technology (Invitrogen) was used in all cloning procedures as previously described (D'Avino et al., 2006). The destination vectors used for the expression in *Drosophila* cultured cells were previously described (D'Avino et al., 2006, 2008, 2009). The pDEST15 vector (Invitrogen) was used for bacterial expression of GST-tagged proteins. To express GFP-tagged Nesd protein in flies, we used destination vectors for *Drosophila* germline transformation containing N- or C-terminal GFP tags and a ubiquitin promoter provided by R. Basto (Institute Curie, Centre National de la Recherche Scientifique, Paris, France; Basto et al., 2008). pDEST53 and pDEST47 (Invitrogen) were used to express GFP-tagged proteins in human cells.

Affinity purification and in vivo pull-down assays

PrA purifications were performed essentially as described previously (D'Avino et al., 2008, 2009). Approximately 10^9 cells were harvested by centrifugation and frozen in liquid nitrogen. The cell pellet was then resuspended in 5 ml of extraction buffer (50 mM Tris-Cl, pH 7.5, 150 mM NaCl, 2 mM $MgCl_2$, 1 mM EGTA, 0.1% NP-40, 1 mM DTT, and protease inhibitors [Complete; Roche]) and homogenized using a high-performance disperser (Power Gen 125; Thermo Fisher Scientific). Homogenates were agitated at 4°C for 30 min and clarified by centrifugation at 8,000 rpm in an SS34 rotor (Beckman Coulter). 200 µl Dynabeads (Invitrogen) conjugated to rabbit IgG (MP Biomedicals) was added to the supernatants and incubated for 4 h under continuous agitation at 4°C. Beads were then washed five times for 10 min in 10 ml of extraction buffer. Proteins were then eluted from beads with 0.5 M NH_4OH and 0.5 mM EDTA, lyophilized, and resuspended in Laemmli SDS-PAGE sample buffer (Sigma-Aldrich). Proteins were separated on 4–20 or 8–16% SDS-PAGE gels, and specific bands were excised and analyzed by liquid chromatography–MS/MS. The MS/MS fragmentation data achieved were used to search the National Center for Biotechnology Information and Flybase databases using the Mascot search engine. Probability-based Mascot scores were used to evaluate identifications. Only matches with $P < 0.05$ for random occurrence were considered significant.

For pull-down assays using *Drosophila* cell extracts, 5×10^7 cells were collected and processed as described in the previous paragraph. Eluates were then fractioned on an 8–16% SDS-PAGE gel, transferred onto a polyvinylidene difluoride membrane, and probed with the antibodies indicated in Figs. 2 (A and G), 5 C, and 6 B.

Immunoprecipitations of human cell extracts were performed essentially as previously described (Petretti et al., 2006). HeLa cells were transfected with pCMV-SHCBP1::GFP for 48 h and then resuspended in lysis buffer (1 mM EGTA, 1 mM $NaVO_4$, 50 mM β-glycerophosphate, 1 mM NaF, 10% glycerol, 1 mM DTT, 150 mM KCl, 50 mM Hepes, pH 7.5, 0.5% NP-40, 1 mM β-mercaptoethanol, 1 mM EDTA, 1 mM $MgCl_2$, and protease inhibitors). Cell extracts were centrifuged at 10,000 *g* for 10 min at 4°C, and supernatants were incubated for 1 h at 4°C with 50 µl protein G Dynabeads (Dynal) coated with anti-GFP antibodies (Roche). Beads were washed three times with lysis buffer and resuspended in 50 µl Laemmli SDS-PAGE sample buffer. Proteins were fractioned on a 10% SDS-PAGE gel, transferred onto a polyvinylidene difluoride membrane, and probed with GFP, MKLP1, and RacGAP1 antibodies.

In vitro binding assay

DNA fragments coding for Nesd, RacGAP50C, or Pav-KLP were generated by PCR and cloned into pDEST15 (Invitrogen) to express N-terminal GST-tagged polypeptides in *Escherichia coli*. The GST-tagged products were then purified using glutathione–Sepharose 4B according to the manufacturer's instruction (GE Healthcare). [^{35}S]Methionine-labeled Nesd, RacGAP50C, or Pav-KLP fragments were prepared from corresponding PCR products amplified using primers harboring a T7 promoter and then transcribed and translated in vitro using the TnT T7 Quick-Coupled Transcription/Translation System (Promega) in the presence of [^{35}S]methionine. Generally, 25 µl glutathione–Sepharose beads containing purified GST proteins was mixed with 5 µl [^{35}S]methionine-labeled polypeptides and 300 µl NET-N$^+$ buffer (50 mM Tris-HCl, pH 7.4, 150 mM NaCl, 5 mM EDTA, 0.5% NP-40, and a cocktail of protease inhibitors) and incubated in ice for 30 min with periodic agitation. The mixture was then washed five times by adding 500 µl NET-N$^+$ buffer followed by centrifugation at 500 *g* for 1 min. Beads were resuspended in 25 µl Laemmli SDS-PAGE sample buffer, and, typically, one fifth of the mixture (10 µl) was loaded on 8–16% Tris-glycine gel. Proteins were then transferred onto a nitrocellulose membrane using the dry blotting system (iBlot; Invitrogen) and exposed to x-ray films at −80°C.

Fly stocks and genetics

Flies were raised on standard maize meal medium at 25°C. The *nesd*^{1} allele corresponds to *y*^{1}*w*^{67c23}*;P{EPgy2}CG10722*^{EY08338} and was obtained from Bloomington. The deficiency *Df(2L)ED1305* was obtained form J. Roote (University of Cambridge, Cambridge, England, UK) and is described in Flybase. The *PLCδ-PH::GFP* and *Sqh::GFP* fly stocks were provided by J. Brill (University of Toronto, Toronto, Canada; Wong et al., 2005) and R. Karess (Institut Jacques Monod, Centre National de la Recherche Scientifique, Paris, France; Royou et al., 2004), respectively. The *GFP::Pav-KLP* stock and the *pav*^{B200} allele were previously described (Adams et al., 1998; Minestrini et al., 2002). *P*-element excision was performed using standard procedures. Transgenic flies were generated by BestGene, Inc.

Identification of Nesd orthologues, sequence alignment, and family tree

Nesd orthologues were identified using the PSI-BLAST program (Altschul et al., 1997) from the National Center for Biotechnology Information blastp suite. After five iterations, 10 out of the 100 sequences with the best E values were selected based on matching description and evolutionary distance of the corresponding species. These were aligned with MUSCLE (Edgar, 2004), trimmed down to the four sequences displayed, and visualized with Jalview. The tree was derived from the 10-species alignment thanks to PhyML (Guindon and Gascuel, 2003) using the LG model.

Ovaries and testes immunostaining

Ovaries were dissected in PBS, fixed with 4% formaldehyde in PBS for 20 min, and then rinsed three times with PBT (PBS with 0.5% Triton X-100). After blocking for 1 h in PBT containing 3% BSA, ovaries were incubated overnight on a rotating wheel at 4°C with primary antibodies diluted in PBT containing 1% BSA. Ovaries were then rinsed three times with PBT and incubated with secondary antibodies and/or phalloidin rhodamine for 3 h on a rotating wheel at room temperature. Ovarioles were then separated and spread under a coverslip with a drop of Vectashield with DAPI (Vector Laboratories).

Testes were dissected from early pupae in PBS as previously described (Pisano et al., 1993) and fixed using either ice-cold methanol for 10 min or ice-cold ethanol for 10 min followed by 10-min incubation in 4% formaldehyde to preserve GFP fluorescence. Incubations with primary antibodies were performed overnight at 4°C in a humid chamber. Preparations were then incubated with secondary antibodies and/or phalloidin rhodamine at room temperature for 2–3 h. Samples were washed with PBS and mounted in Vectashield with DAPI.

Antibodies

Antibodies were raised in guinea pigs against a full-length His-tagged Nesd protein expressed and purified using a baculovirus system. Serum production was performed by Harlan. Other antibodies used in this study were mouse monoclonal antitubulin (clone DM1A; Sigma-Aldrich), rabbit anti–Pav-KLP (Minestrini et al., 2002), rabbit anti-RacGAP50C (D'Avino et al., 2006), rabbit anti-Anillin (Field and Alberts, 1995), monoclonal mouse anti-myc (clone 9E10; Santa Cruz Biotechnology, Inc.), mouse monoclonal anti-GFP (Roche), goat anti-RacGAP1 (Abcam), rabbit anti-MKLP1 (clone

N-19; Santa Cruz Biotechnology, Inc.), mouse monoclonal anti-Hts (clone RC; Developmental Studies Hybridoma Bank), mouse monoclonal anti-spectrin (clone 3A9; Developmental Studies Hybridoma Bank), Peroxidase-ChromPure anti–rabbit IgG (Jackson ImmunoResearch Laboratories, Inc.), and rhodamine phalloidin (Invitrogen). Peroxidase- and Alexa Fluor–conjugated secondary antibodies were purchased from Jackson ImmunoResearch Laboratories, Inc.

Microscopy

Fixed HeLa and Dmel cells were visualized on a fluorescence microscope (Axiovert 200; Carl Zeiss, Inc.) with a 100× NA 1.4 objective and acquired using a camera (Coolsnap HQ; Photometrics) and Metamorph software (MDS Analytical Technologies). Fixed testes and ovaries were visualized on a confocal microscope (LSM510 Meta; Carl Zeiss, Inc.) with two different objectives: 100× NA 1.4 and 40× NA 1.3. Time-lapse imaging analyses of primary spermatocytes were performed using a 100× NA 1.4 objective on a fluorescence microscope outfitted with excitation, emission, and neutral density filter wheels (Prior Scientific) and a z-axis focus drive (PIFOC; Physik Instruments). Samples were maintained at a constant temperature of 25°C throughout filming. Images were acquired using a Coolsnap HQ camera and Metamorph software. All images were analyzed using ImageJ (National Institutes of Health) and processed in Photoshop (Adobe).

Glycan array screen

Baculovirus-expressed His-tagged full-length Nesd was diluted to 200 µg/ml in TSM buffer (20 mM Tris-Hcl, pH 7.4, 150 mM NaCl, 2 mM $CaCl_2$, and 2 mM $MgCl_2$) with the additions of 1% BSA, 0.05% Tween 20, and 2 mM β-mercaptoethanol. 70 µl was applied to the printed surface of the array, coverslipped, and incubated at room temperature in a humidified chamber for 1 h. The coverslip was then removed, and the slide was rinsed four times each in TSM buffer + 0.05% Tween 20. Secondary incubation was performed with rabbit anti-His antibody (sc803; Santa Cruz Biotechnology, Inc.) at 5 µg/ml in TSM buffer for 1 h in a humidified chamber. Binding was detected by incubating the slide for 1 h in a humidified chamber in the dark with Alexa Fluor 488 anti–rabbit IgG diluted in TSM buffer. The coverslip was then removed, and the slide was rinsed four times in TSM and then in water. The slide was then spun dry and scanned for analysis (full details are also described at the CFG website).

Online supplemental material

Fig. S1 shows in vitro pull-down of Nesd by GST-tagged RacGAP50C and Pav-KLP, specificity of Nesd antibody, and colocalization of Nesd and RacGAP50C at the midbody in cultured cells. Fig. S2 shows interaction of PrA::Pav-KLP with myc-tagged Nesd fragments in cultured cells and normal localization of RacGAP50C and Pav-KLP in *nesd* RNAi cells. Fig. S3 shows that SHCBP1 RNAi does not impair cytokinesis in HeLa cells. Fig. S4 illustrates the levels of expression of various Nesd::GFP transgenes, cytokinesis in *nesd*^{1}*/Df;GFP::pav* animals, and Pav-KLP localization during anaphase in primary spermatocytes. Fig. S5 shows Nesd::GFP localization to ring canals and fusomes in primary spermatocytes and egg chambers. Video 1 shows cytokinesis in a *wild-type* spermatocyte expressing a Sqh::GFP transgene. Video 2 shows cytokinesis in a *nesd* mutant spermatocyte expressing a Sqh::GFP transgene. Video 3 illustrates Nesd::GFP dynamics during spermatocyte cytokinesis. Online supplemental material is available at http://www.jcb.org/cgi/content/full/jcb.201007060/DC1.

We thank T. Minns for technical assistance and G. Callaini for technical advice. We are particularly grateful to M. Savoian for technical advice on time-lapse imaging and for critical reading of the manuscript. We also thank R. Basto, J. Brill, R. Karess, J. Roote, the Bloomington Stock Center, and the Developmental Studies Hybridoma Bank for fly stocks and reagents. We would also like to thank two anonymous reviewers for helpful comments and for pointing out that Pav-KLP stained the Y-chromosome loop in Fig. S5 A. The authors would like to acknowledge the Protein-Glycan Interaction Core (H) of the CFG funded by the National Institute of General Medical Sciences (GM62116) for the glycan array analysis.

This work was supported by a Cancer Research UK project grant to P.P. D'Avino, a Cancer Research UK program grant to D.M. Glover, and a Biotechnology and Biological Sciences Research Council project grant to D.M. Glover, E.D. Laue, and P.P. D'Avino. E.D. Laue would like to thank the Wellcome Trust for support.

Submitted: 12 July 2010
Accepted: 29 November 2010

References

Adams, R.R., A.A. Tavares, A. Salzberg, H.J. Bellen, and D.M. Glover. 1998. *pavarotti* encodes a kinesin-like protein required to organize the central spindle and contractile ring for cytokinesis. *Genes Dev.* 12:1483–1494. doi:10.1101/gad.12.10.1483

Altschul, S.F., T.L. Madden, A.A. Schäffer, J. Zhang, Z. Zhang, W. Miller, and D.J. Lipman. 1997. Gapped BLAST and PSI-BLAST: a new generation of protein database search programs. *Nucleic Acids Res.* 25:3389–3402. doi:10.1093/nar/25.17.3389

Basto, R., K. Brunk, T. Vinadogrova, N. Peel, A. Franz, A. Khodjakov, and J.W. Raff. 2008. Centrosome amplification can initiate tumorigenesis in flies. *Cell.* 133:1032–1042. doi:10.1016/j.cell.2008.05.039

Benton, R., I.M. Palacios, and D. St Johnston. 2002. *Drosophila* 14-3-3/PAR-5 is an essential mediator of PAR-1 function in axis formation. *Dev. Cell.* 3:659–671. doi:10.1016/S1534-5807(02)00320-9

D'Avino, P.P., M.S. Savoian, and D.M. Glover. 2005. Cleavage furrow formation and ingression during animal cytokinesis: a microtubule legacy. *J. Cell Sci.* 118:1549–1558. doi:10.1242/jcs.02335

D'Avino, P.P., M.S. Savoian, L. Capalbo, and D.M. Glover. 2006. RacGAP50C is sufficient to signal cleavage furrow formation during cytokinesis. *J. Cell Sci.* 119:4402–4408. doi:10.1242/jcs.03210

D'Avino, P.P., T. Takeda, L. Capalbo, W. Zhang, K.S. Lilley, E.D. Laue, and D.M. Glover. 2008. Interaction between Anillin and RacGAP50C connects the actomyosin contractile ring with spindle microtubules at the cell division site. *J. Cell Sci.* 121:1151–1158. doi:10.1242/jcs.026716

D'Avino, P.P., V. Archambault, M.R. Przewloka, W. Zhang, E.D. Laue, and D.M. Glover. 2009. Isolation of protein complexes involved in mitosis and cytokinesis from *Drosophila* cultured cells. *Methods Mol. Biol.* 545:99–112. doi:10.1007/978-1-60327-993-2_6

de Cuevas, M., M.A. Lilly, and A.C. Spradling. 1997. Germline cyst formation in *Drosophila*. *Annu. Rev. Genet.* 31:405–428. doi:10.1146/annurev.genet.31.1.405

Douglas, M.E., T. Davies, N. Joseph, and M. Mishima. 2010. Aurora B and 14-3-3 coordinately regulate clustering of centralspindlin during cytokinesis. *Curr. Biol.* 20:927–933. doi:10.1016/j.cub.2010.03.055

Edgar, R.C. 2004. MUSCLE: multiple sequence alignment with high accuracy and high throughput. *Nucleic Acids Res.* 32:1792–1797. doi:10.1093/nar/gkh340

Eggert, U.S., T.J. Mitchison, and C.M. Field. 2006. Animal cytokinesis: from parts list to mechanisms. *Annu. Rev. Biochem.* 75:543–566. doi:10.1146/annurev.biochem.74.082803.133425

Field, C.M., and B.M. Alberts. 1995. Anillin, a contractile ring protein that cycles from the nucleus to the cell cortex. *J. Cell Biol.* 131:165–178. doi:10.1083/jcb.131.1.165

Fuller, M.T. 1993. Spermatogenesis. *In* The Development of *Drosophila melanogaster*. Vol. 1. M. Bate and A.M. Arias, editors. Cold Spring Harbor Laboratory Press, Plainview, NY. 71–148.

Giansanti, M.G., S. Bonaccorsi, E. Bucciarelli, and M. Gatti. 2001. *Drosophila* male meiosis as a model system for the study of cytokinesis in animal cells. *Cell Struct. Funct.* 26:609–617. doi:10.1247/csf.26.609

Giansanti, M.G., R.M. Farkas, S. Bonaccorsi, D.L. Lindsley, B.T. Wakimoto, M.T. Fuller, and M. Gatti. 2004. Genetic dissection of meiotic cytokinesis in *Drosophila* males. *Mol. Biol. Cell.* 15:2509–2522. doi:10.1091/mbc.E03-08-0603

Goshima, G., and R.D. Vale. 2003. The roles of microtubule-based motor proteins in mitosis: comprehensive RNAi analysis in the *Drosophila* S2 cell line. *J. Cell Biol.* 162:1003–1016. doi:10.1083/jcb.200303022

Greenbaum, M.P., L. Ma, and M.M. Matzuk. 2007. Conversion of midbodies into germ cell intercellular bridges. *Dev. Biol.* 305:389–396. doi:10.1016/j.ydbio.2007.02.025

Gregory, S.L., S. Ebrahimi, J. Milverton, W.M. Jones, A. Bejsovec, and R. Saint. 2008. Cell division requires a direct link between microtubule-bound RacGAP and Anillin in the contractile ring. *Curr. Biol.* 18:25–29. doi:10.1016/j.cub.2007.11.050

Guindon, S., and O. Gascuel. 2003. A simple, fast, and accurate algorithm to estimate large phylogenies by maximum likelihood. *Syst. Biol.* 52:696–704. doi:10.1080/10635150390235520

Hart, G.W., M.P. Housley, and C. Slawson. 2007. Cycling of O-linked beta-N-acetylglucosamine on nucleocytoplasmic proteins. *Nature.* 446:1017–1022. doi:10.1038/nature05815

Hime, G.R., J.A. Brill, and M.T. Fuller. 1996. Assembly of ring canals in the male germ line from structural components of the contractile ring. *J. Cell Sci.* 109:2779–2788.

Hirose, K., T. Kawashima, I. Iwamoto, T. Nosaka, and T. Kitamura. 2001. MgcRacGAP is involved in cytokinesis through associating with mitotic spindle and midbody. *J. Biol. Chem.* 276:5821–5828. doi:10.1074/jbc.M007252200

Inoue, Y.H., M.S. Savoian, T. Suzuki, E. Máthé, M.T. Yamamoto, and D.M. Glover. 2004. Mutations in *orbit/mast* reveal that the central spindle is comprised of two microtubule populations, those that initiate cleavage and those that propagate furrow ingression. *J. Cell Biol.* 166:49–60. doi:10.1083/jcb.200402052

Koch, E.A., and R.C. King. 1969. Further studies on the ring canal system of the ovarian cystocytes of *Drosophila melanogaster*. *Z. Zellforsch. Mikrosk. Anat.* 102:129–152. doi:10.1007/BF00336421

Kramerov, A.A., N.P. Arbatsky, Y.M. Rozovsky, E.A. Mikhaleva, O.O. Polesskaya, V.A. Gvozdev, and V.N. Shibaev. 1996. Mucin-type glycoprotein from *Drosophila melanogaster* embryonic cells: characterization of carbohydrate component. *FEBS Lett.* 378:213–218. doi:10.1016/0014-5793(95)01444-6

Kramerova, I.A., and A.A. Kramerov. 1999. Mucinoprotein is a universal constituent of stable intercellular bridges in *Drosophila melanogaster* germ line and somatic cells. *Dev. Dyn.* 216:349–360. doi:10.1002/(SICI)1097-0177(199912)216:4/5<349::AID-DVDY4>3.0.CO;2-X

Matuliene, J., and R. Kuriyama. 2002. Kinesin-like protein CHO1 is required for the formation of midbody matrix and the completion of cytokinesis in mammalian cells. *Mol. Biol. Cell.* 13:1832–1845. doi:10.1091/mbc.01-10-0504

Mayans, O., M. Scott, I. Connerton, T. Gravesen, J. Benen, J. Visser, R. Pickersgill, and J. Jenkins. 1997. Two crystal structures of pectin lyase A from *Aspergillus* reveal a pH driven conformational change and striking divergence in the substrate-binding clefts of pectin and pectate lyases. *Structure.* 5:677–689. doi:10.1016/S0969-2126(97)00222-0

Minestrini, G., E. Máthé, and D.M. Glover. 2002. Domains of the Pavarotti kinesin-like protein that direct its subcellular distribution: effects of mislocalisation on the tubulin and actin cytoskeleton during *Drosophila* oogenesis. *J. Cell Sci.* 115:725–736.

Mishima, M., S. Kaitna, and M. Glotzer. 2002. Central spindle assembly and cytokinesis require a kinesin-like protein/RhoGAP complex with microtubule bundling activity. *Dev. Cell.* 2:41–54. doi:10.1016/S1534-5807(01)00110-1

Montembault, E., S. Dutertre, C. Prigent, and R. Giet. 2007. PRP4 is a spindle assembly checkpoint protein required for MPS1, MAD1, and MAD2 localization to the kinetochores. *J. Cell Biol.* 179:601–609. doi:10.1083/jcb.200703133

North, S.J., K. Koles, C. Hembd, H.R. Morris, A. Dell, V.M. Panin, and S.M. Haslam. 2006. Glycomic studies of *Drosophila melanogaster* embryos. *Glycoconj. J.* 23:345–354. doi:10.1007/s10719-006-6693-4

Otegui, M.S., K.J. Verbrugghe, and A.R. Skop. 2005. Midbodies and phragmoplasts: analogous structures involved in cytokinesis. *Trends Cell Biol.* 15:404–413. doi:10.1016/j.tcb.2005.06.003

Pavicic-Kaltenbrunner, V., M. Mishima, and M. Glotzer. 2007. Cooperative assembly of CYK-4/MgcRacGAP and ZEN-4/MKLP1 to form the centralspindlin complex. *Mol. Biol. Cell.* 18:4992–5003. doi:10.1091/mbc.E07-05-0468

Petretti, C., M. Savoian, E. Montembault, D.M. Glover, C. Prigent, and R. Giet. 2006. The PITSLRE/CDK11p58 protein kinase promotes centrosome maturation and bipolar spindle formation. *EMBO Rep.* 7:418–424.

Pisano, C., S. Bonaccorsi, and M. Gatti. 1993. The kl-3 loop of the Y chromosome of *Drosophila melanogaster* binds a tektin-like protein. *Genetics.* 133:569–579.

Prekeris, R., and G.W. Gould. 2008. Breaking up is hard to do - membrane traffic in cytokinesis. *J. Cell Sci.* 121:1569–1576. doi:10.1242/jcs.018770

Robinson, D.N., and L. Cooley. 1996. Stable intercellular bridges in development: the cytoskeleton lining the tunnel. *Trends Cell Biol.* 6:474–479. doi:10.1016/0962-8924(96)84945-2

Royou, A., C. Field, J.C. Sisson, W. Sullivan, and R. Karess. 2004. Reassessing the role and dynamics of nonmuscle myosin II during furrow formation in early *Drosophila* embryos. *Mol. Biol. Cell.* 15:838–850. doi:10.1091/mbc.E03-06-0440

Schmandt, R., S.K. Liu, and C.J. McGlade. 1999. Cloning and characterization of mPAL, a novel Shc SH2 domain-binding protein expressed in proliferating cells. *Oncogene.* 18:1867–1879. doi:10.1038/sj.onc.1202507

Simon, G.C., E. Schonteich, C.C. Wu, A. Piekny, D. Ekiert, X. Yu, G.W. Gould, M. Glotzer, and R. Prekeris. 2008. Sequential Cyk-4 binding to ECT2 and FIP3 regulates cleavage furrow ingression and abscission during cytokinesis. *EMBO J.* 27:1791–1803. doi:10.1038/emboj.2008.112

Slawson, C., N.E. Zachara, K. Vosseller, W.D. Cheung, M.D. Lane, and G.W. Hart. 2005. Perturbations in O-linked beta-N-acetylglucosamine protein modification cause severe defects in mitotic progression and cytokinesis. *J. Biol. Chem.* 280:32944–32956. doi:10.1074/jbc.M503396200

Somers, W.G., and R. Saint. 2003. A RhoGEF and Rho family GTPase-activating protein complex links the contractile ring to cortical microtubules at the onset of cytokinesis. *Dev. Cell.* 4:29–39. doi:10.1016/S1534-5807(02)00402-1

Somma, M.P., B. Fasulo, G. Cenci, E. Cundari, and M. Gatti. 2002. Molecular dissection of cytokinesis by RNA interference in *Drosophila* cultured cells. *Mol. Biol. Cell.* 13:2448–2460. doi:10.1091/mbc.01-12-0589

Spradling, A.C. 1993. Developmental Genetics of Oogenesis. *In* The Development of *Drosophila melanogaster*. Vol. 1. M. Bate and A.M. Arias, editors. Cold Spring Harbor Laboratory Press, Plainview, NY. 1–70.

Tilney, L.G., M.S. Tilney, and G.M. Guild. 1996. Formation of actin filament bundles in the ring canals of developing *Drosophila* follicles. *J. Cell Biol.* 133:61–74. doi:10.1083/jcb.133.1.61

Wang, H., A. Spang, M.A. Sullivan, J. Hryhorenko, and F.K. Hagen. 2005. The terminal phase of cytokinesis in the *Caenorhabditis elegans* early embryo requires protein glycosylation. *Mol. Biol. Cell.* 16:4202–4213. doi:10.1091/mbc.E05-05-0472

Wang, Z., N.D. Udeshi, C. Slawson, P.D. Compton, K. Sakabe, W.D. Cheung, J. Shabanowitz, D.F. Hunt, and G.W. Hart. 2010. Extensive crosstalk between O-GlcNAcylation and phosphorylation regulates cytokinesis. *Sci. Signal.* 3:ra2. doi:10.1126/scisignal.2000526

Wong, R., I. Hadjiyanni, H.C. Wei, G. Polevoy, R. McBride, K.P. Sem, and J.A. Brill. 2005. PIP2 hydrolysis and calcium release are required for cytokinesis in *Drosophila* spermatocytes. *Curr. Biol.* 15:1401–1406. doi:10.1016/j.cub.2005.06.060

Xue, F., and L. Cooley. 1993. *Kelch* encodes a component of intercellular bridges in *Drosophila* egg chambers. *Cell.* 72:681–693. doi:10.1016/0092-8674(93)90397-9

Yüce, O., A. Piekny, and M. Glotzer. 2005. An ECT2–centralspindlin complex regulates the localization and function of RhoA. *J. Cell Biol.* 170:571–582. doi:10.1083/jcb.200501097

Yue, L., and A.C. Spradling. 1992. hu-li tai shao, a gene required for ring canal formation during *Drosophila* oogenesis, encodes a homolog of adducin. *Genes Dev.* 6:2443–2454. doi:10.1101/gad.6.12b.2443

Zhang, L., and K.G. Ten Hagen. 2010. Dissecting the biological role of mucin-type O-glycosylation using RNA interference in *Drosophila* cell culture. *J. Biol. Chem.* 285:34477–34484.

Zhao, W.M., A. Seki, and G. Fang. 2006. Cep55, a microtubule-bundling protein, associates with centralspindlin to control the midbody integrity and cell abscission during cytokinesis. *Mol. Biol. Cell.* 17:3881–3896. doi:10.1091/mbc.E06-01-0015